Electronic Supplementary Information for

Compressible AgNWs/$Ti_3C_2T_X$ MXene Aerogel-based Highly Sensitive Piezoresistive Pressure Sensor as Versatile Electronic Skins

Lili Bi, Zhonglin Yang, Liangjun Chen, Zhen Wu, Cui Ye*

College of Materials Science and Engineering, Zhejiang University of Technology, Hangzhou 310014, China

**Corresponding authors. E-mail: ye0702@zjut.edu.cn (C. Y.)*

Materials. $AgNO_3$, NaCl, NaBr, ethylene glycol (EG) were obtained from Sinopharm Chemical Reagent Co. Ltd. Polyvinyl pyrrolidone (PVP, 36 w) were received from Sigma-Aldrich. Fluorocarbon surfactant (TF281) was obtained from Shanghai Futian Chemicals. Hydrochloric acid (HCl, 36.5 %) and calciumfluoride ($CaCl_2$, AR) were purchased from Chengdu Kelong Chemcial Inc. Lithium fluoride (LiF, AR) and SA (AR) was purchased from Aladdin Inc. Ti_3AlC_2 powder (400 mesh) was purchased from Laizhou Kai Kai Ceramic Materials Co. Ltd. PDMS is Dow Corning 184. deionized (DI) water (18.2 MΩ cm) was produced using an ultrapure water system (GWB-1). Filtration membranes (pore size of 8 μm) were obtained from Tiantai Zhongli Filter Equipment Factory Co. Ltd. All chemicals were analytical reagents and used as received without further purification.

Synthesis of AgNWs. AgNWs were synthesized by the polyol reduction according to our previous work[S1]. And AgNWs raw product (130 mL) was purified by dynamic agitation cleaning according to our previously published work[S2]. In this case, filtration membrane of the purification facility is with a pore diameter of 8 μm, and the stirring speed of a six-hole stirring paddle was 900 rpm. DI water containing surfactants was dropped into the chamber of purification facility to maintain a constant volume of AgNWs ink for a certain time, ensuring the final AgNWs ink is concentrated to a specific concentration (5 mg mL^{-1}) for subsequent experiments.

Synthesis of $Ti_3C_2T_x$. $Ti_3C_2T_x$ suspensions were prepared through etching Ti_3AlC_2 powder in 9 mL hydrochloric acid (HCl) aqueous solution containing dissolved LiF salt (Ti_3AlC_2: LiF = 1:1 (wt/wt)). The etching solution was stirred at a constant temperature of 35 °C for 24 h. Following the etching, the $Ti_3C_2T_x$ sediment was washed using deionized (DI) water, followed by centrifugation (3500 rpm, 5 min) until the pH of the supernatant was nearly neutral (pH ≈ 6). Then, the deposition was redispersed in DI water and sonicated for 20 min under N_2 flow protection, followed by centrifugation at 7500 rpm for 20 min. The $Ti_3C_2T_x$ nanosheets derived from the supernatant was used in the work.

Calculation procedure. A detailed calculation process of 50 μL water drop approximately equaling to 1.25 Pa applied pressure is presented below:

The mass of a water drop (50 μL) is calculated as below:

$$m = \left(50 \times 10^{-3} \times 1\right) g = 0.05\ g$$

g presents Gravitational acceleration (10 N/Kg, approximate calculation is made here). Our pressure sensor is a cubic structure with a side length of 2 cm, and the pressure exerted on the pressure sensor by a 50 μL water drop is calculated below:

$$p\left(Pa, N/m^2\right) = \frac{F}{s} = \frac{mg}{s} = \frac{0.05 \times 10 \times 10^{-3}}{2 \times 2 \times 10^{-4}} = 1.25\ (Pa)$$

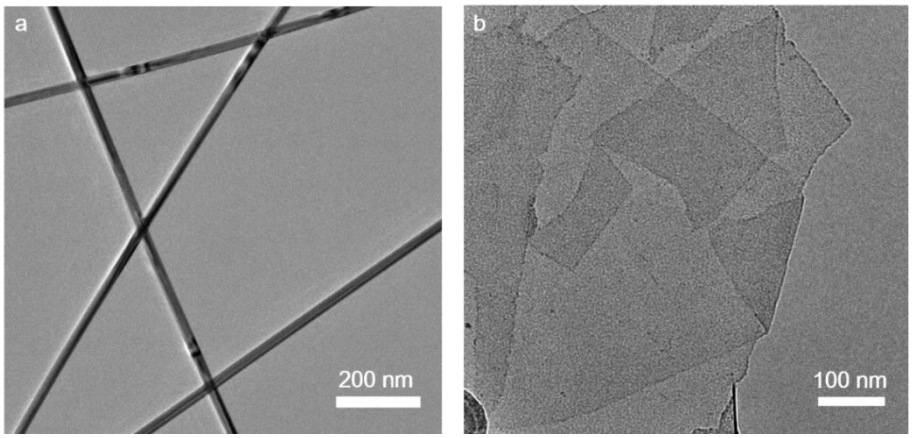

Fig. S1. TEM images of (a) AgNWs and (b) $Ti_3C_2T_x$.

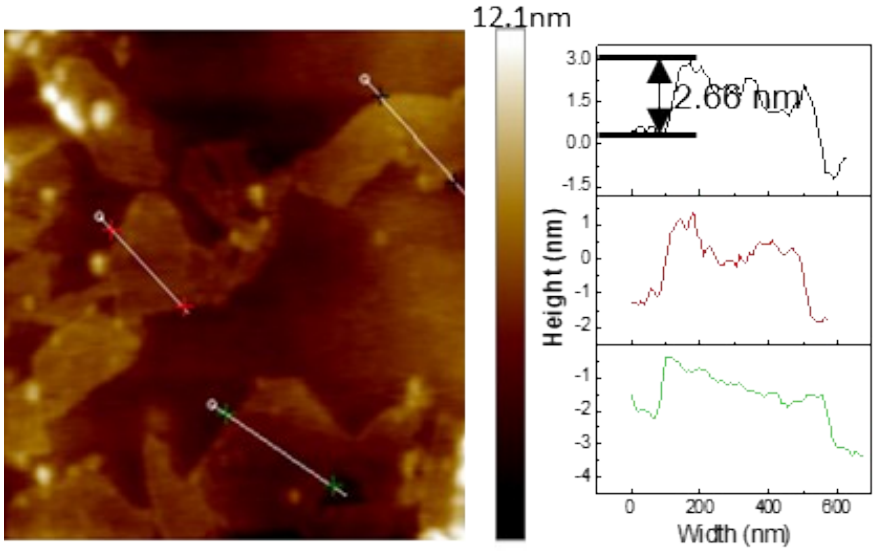

Fig. S2. AFM image of $Ti_3C_2T_x$.

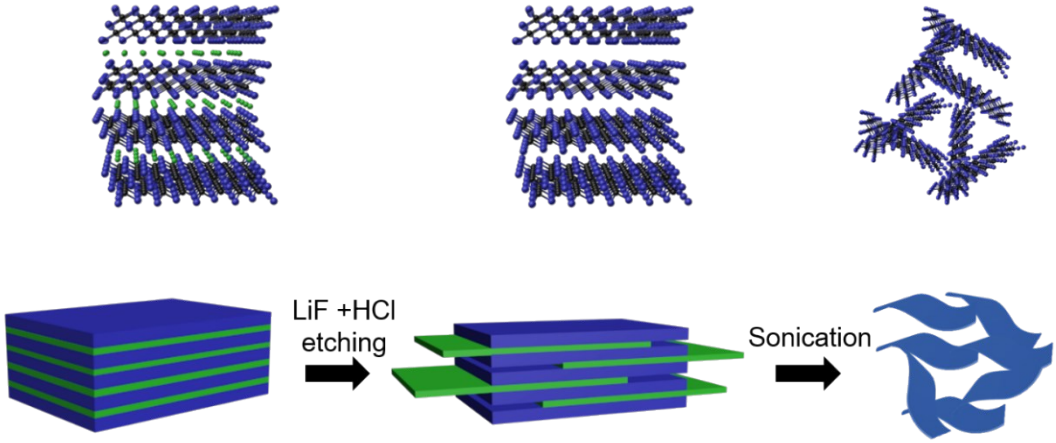

Fig. S3. Schematic illustration of the preparation process of $Ti_3C_2T_x$.

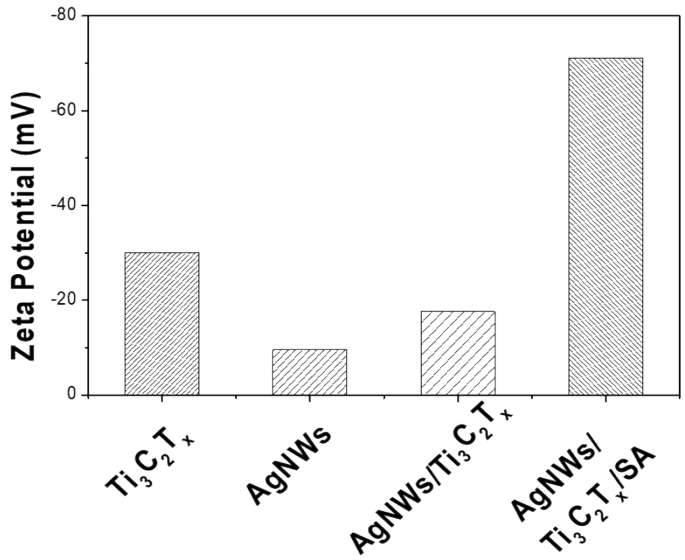

Fig. S4. The Zeta potentials of AgNWs, $Ti_3C_2T_x$, AgNWs/$Ti_3C_2T_x$ and AgNWs/$Ti_3C_2T_x$/SA.

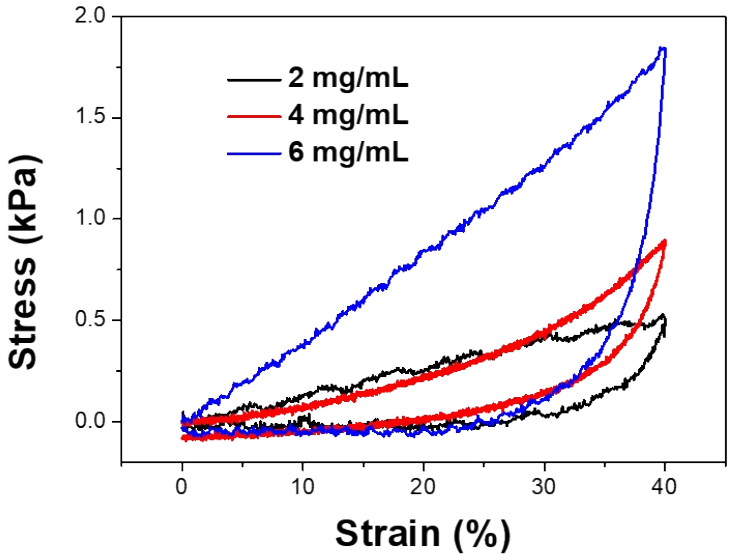

Fig. S5. Stress-strain curves of AgNWs/$Ti_3C_2T_x$ aerogels with different concentration of $CaCl_2$.

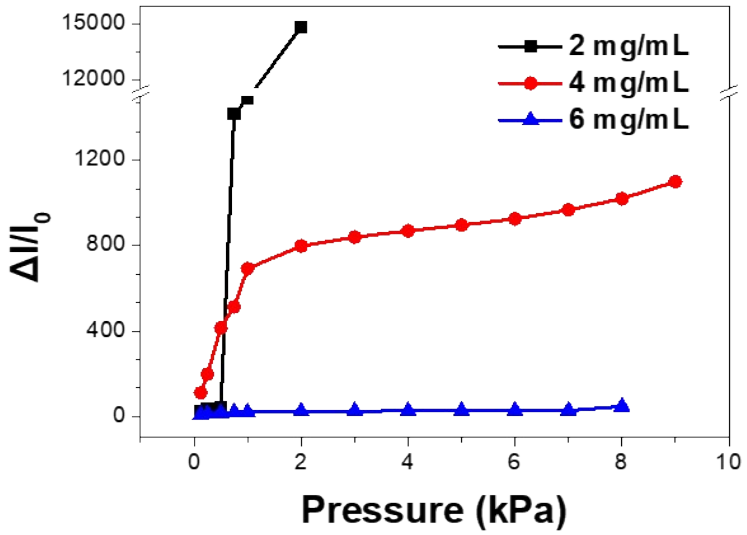

Fig. S6. Linear sensitivity of AgNWs/$Ti_3C_2T_x$ aerogels with different concentration of $CaCl_2$.

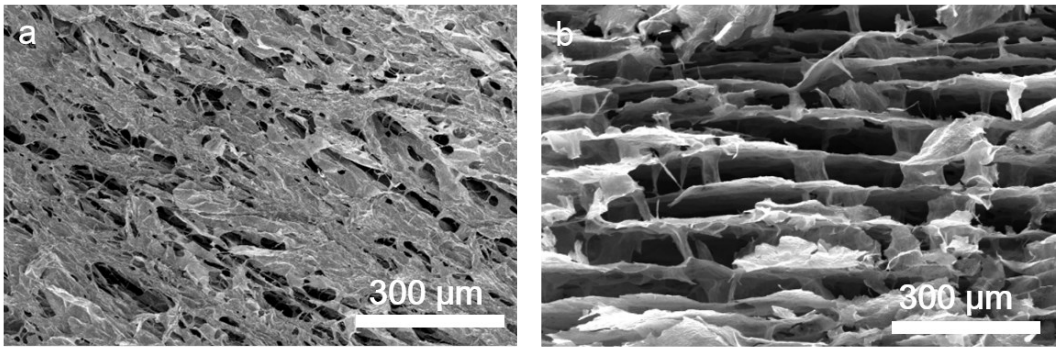

Fig. S7. SEM images of as-prepared AgNWs/$Ti_3C_2T_x$ aerogel fabricated by (a) direct freezing, and (b) directional freezing.

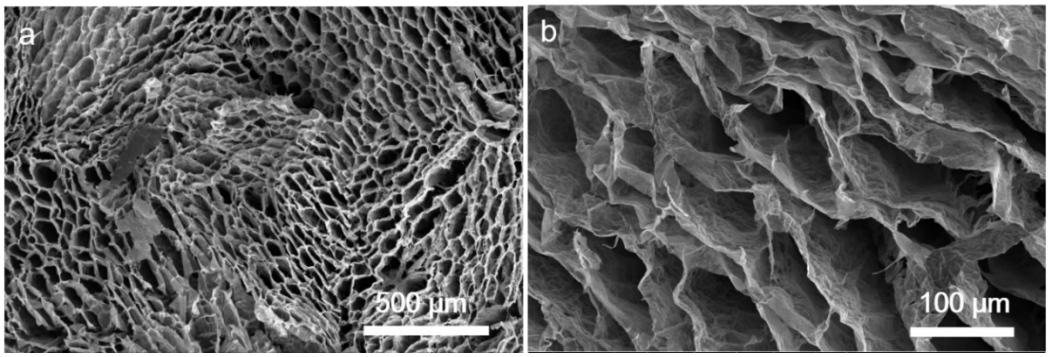

Fig. S8. Top-view SEM images of as-prepared AgNWs/$Ti_3C_2T_x$ aerogel: (a) low-resolution, and (b) high-resolution.

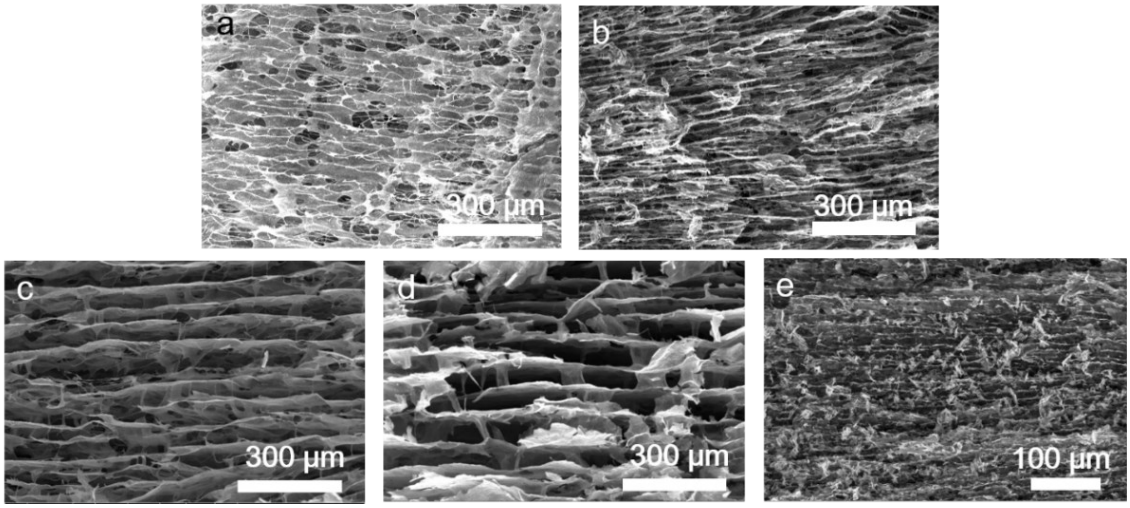

Fig. S9. Side-view SEM images of aerogels with different mass ratios (m/m = AgNWs : $Ti_3C_2T_x$) of (a) 1:0, (b) 2:1, (c) 1:1, (d) 1:2, and (e) 0:1.

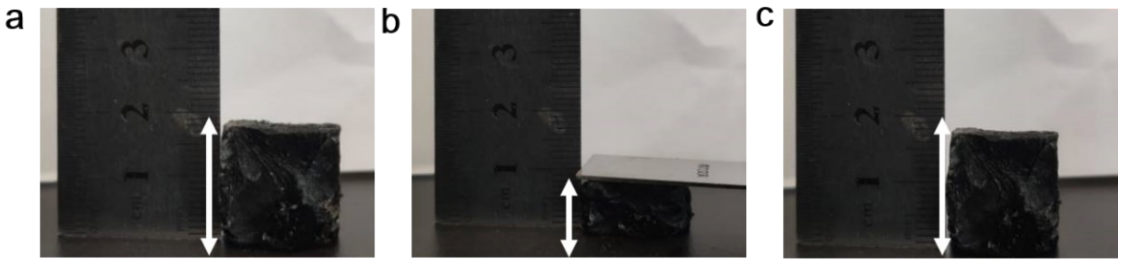

Fig. S10. Manual compression and recovery process of as-prepared AgNWs/$Ti_3C_2T_x$ aerogel.

Fig. S11. The linearity of the proposed piezoresistive pressure sensor.

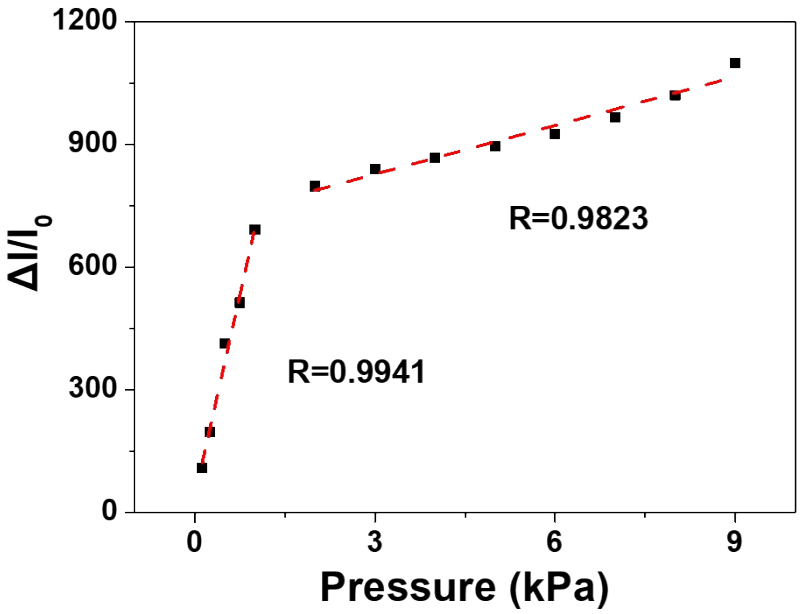

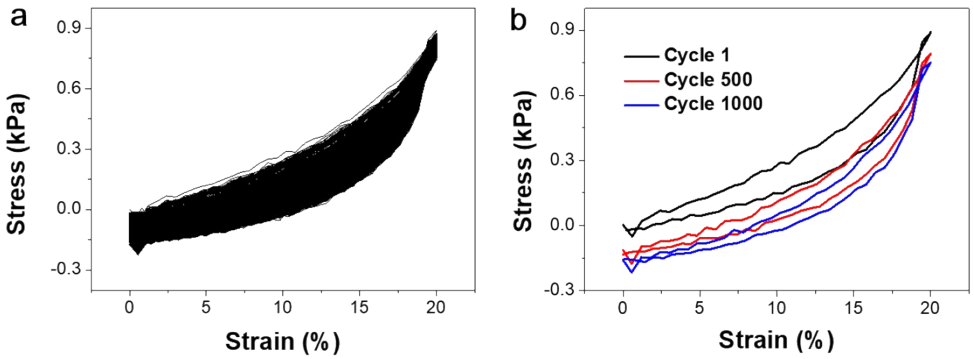

Fig. S12. Stress-strain curves of as-prepared AgNWs/$Ti_3C_2T_x$ aerogel (a) under 1000 compression cycles, and (b) in cycles 1, 500, 1000 of (a).

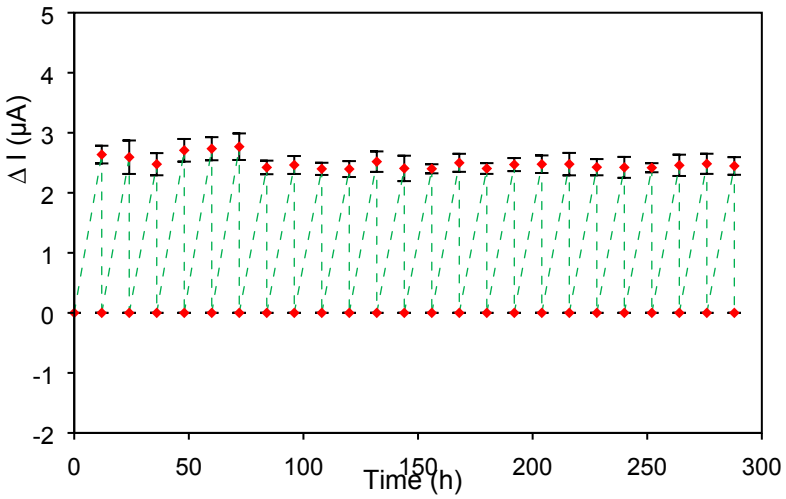

Fig. S13. Long-term durability of the proposed piezoresistive pressure sensor.

Table S1. Comparison of performance of proposed piezoresistive pressure sensor with reported research.

Pressure Sensor	Response time (ms)	Detection limit (Pa)	Sensitivity 1 (detection range)	Sensitivity 2 (detection range)	Ref.
MXene cellulose Aerogel	189	1.0	114.6 kPa^{-1} (0-10 Pa)	45.5 kPa^{-1} (0-10 kPa)	S3
MXene/chitosan Aerogel	109.6	1.0	21.5 kPa^{-1} (0-10 Pa)	80.4 kPa^{-1} (0-10 kPa)	S4
MXene/GO Aerogel	<200	<10	4.05 kPa^{-1} (0-1 kPa)	22.56 kPa^{-1} (1.25-3.5 kPa)	S5
GO Block	N/A	N/A	229.8 kPa^{-1} (0-0.01 kPa)	26.86 kPa^{-1} (0.3-1 kPa)	S6
CuNW/PVA Aerogel	N/A	N/A	0.036 kPa^{-1} (0-4 kPa)	0.003 kPa^{-1} (4-10 kPa)	S7
Aligned pores film	50	2.0	0.6 kPa^{-1} (0-1 kPa)	0.11 kPa^{-1} (1-5 kPa)	S8
PVA/GO film	N/A	2.24	4.52 kPa^{-1} (0-4 kPa)	28.34 kPa^{-1} (4-10 k Pa)	S9
Carbon foam	N/A	3	100.29 kPa^{-1} (0-2 kPa)	21.22 kPa^{-1} (2-10 kPa)	S10
$Ti_3C_2T_x$/BC Aerogel	167	1.0	12.5 kPa^{-1} (0-10 kPa)	N/A	S11
Graphene foam	N/A	N/A	0.36 kPa^{-1} (0-2 kPa)	0.046 kPa^{-1} (2-5 kPa)	S12
PANI/PDMS foam	60	4.0	0.055 kPa^{-1} (0-5 kPa)	N/A	S13
PANI/BC/CH aerogel	N/A	32	1.41 kPa^{-1} (0-1 kPa)	0.31kPa^{-1} (1-2 kPa)	S14
GO/CNT Aerogel	N/A	28	1.22 kPa^{-1} (0-2 kPa)	0.39 kPa^{-1} (2-7 kPa)	S15
GO/CNC Aerogel	N/A	0.875	86.41 kPa^{-1} (0-3.5 kPa)	N/A	S16
AgNWs/$Ti_3C_2T_x$ aerogel	60	1.25	358.57 kPa^{-1} (0-2 kPa)	50.99 kPa^{-1} (2-7 kPa)	This work

REFERENCES

S1 G. Chen, G. Wang, Y. Gu, Z. Wu and C. Ye, CrystEngComm, 2019, **21**, 5243-5248.

S2 G. Chen, L. Bi, Z. Yang, L. Chen, G. Wang and C. Ye, ACS Appl. Mater. Interfaces, 2019, **11**, 22648-22654.

S3 H. Zhuo, Y. Hu, Z. Chen, X. Peng, L. Liu, Q. Luo, J. Yi, C. Liu and L. Zhong, J. Mater. Chem. A, 2019, **7**, 8092-8100.

S4 Y. Hu, H. Zhuo, Q. Luo, Y. Wu, R. Wen, Z. Chen, L. Liu, L. Zhong, X. Peng and R. Sun, J. Mater. Chem. A, 2019, **7**, 10273-10281.

S5 Y. Ma, Y. Yue, H. Zhang, F. Cheng, W. Zhao, J. Rao, S. Luo, J. Wang, X. Jiang, Z. Liu, N. Liu and Y. Gao, ACS Nano, 2018, **12**, 3209-3216.

S6 L. Lv, P. Zhang, T. Xu and L. Qu, ACS Appl. Mater. Interfaces, 2017, **9**, 22885-22892.

S7 Y. Tang, S. Gong, Y. Chen, L. W. Yap and W. Cheng, ACS Nano, 2014, **8**, 5707-5714.

S8 V. V. Sharma, K. N. Kim, G. H. Han, E. J. Gwak, J. H. Woo, S. B. Kang, K. J. Choi, J. Y. Kim and J. M. Baik, Adv. Mater. Technol., 2020, DOI: 10.1002/admt.201901041.

S9 W. Liu, N. Liu, Y. Yue, J. Rao, F. Cheng, J. Su, Z. Liu and Y. Gao, Small, 2018, **14**, e1704149.

S10 W. Liu, N. Liu, Y. Yue, J. Rao, C. Luo, H. Zhang, C. Yang, J. Su, Z. Liu and Y. Gao, J. Mater. Chem. C, 2018, **6**, 1451-1458.

S11 Z. Chen, Y. Hu, H. Zhuo, L. Liu, S. Jing, L. Zhong, X. Peng and R.-c. Sun, Chem. Mater., 2019, **31**, 3301-3312.

S12 J. Liang, Z. Zhao, Y. Tang, X. Hao, X. Wang and J. Qiu, Carbon, 2019, **147**, 206-213.

S13 S. Zheng, X. Wu, Y. Huang, Z. Xu, W. Yang, Z. Liu, S. Huang, B. Xie and M. Yang, Appl. Sci. Manuf., 2019, **121**, 510-516.

S14 J. Huang, D. Li, M. Zhao, H. Ke, A. Mensah, P. Lv, X. Tian and Q. Wei, Chem. Eng. J., 2019, **373**, 1357-1366.

S15 X. Wu, X. Liu, J. Wang, J. Huang and S. Yang, ACS Appl Mater Interfaces, 2018, **10**, 39009-39017.

S16 K. Zhou, C. Chen, M. Lei, Q. Gao, S. Nie, X. Liu and S. Wang, RSC Adv. 2020, **10**, 2150-2159.